Effect of strongly coupled plasma on photoionization cross section

Madhusmita Das

Citation: Physics of Plasmas (1994-present) **21**, 012709 (2014); doi: 10.1063/1.4862550
View online: http://dx.doi.org/10.1063/1.4862550
View Table of Contents: http://scitation.aip.org/content/aip/journal/pop/21/1?ver=pdfcov
Published by the AIP Publishing

Effect of strongly coupled plasma on photoionization cross section

Madhusmita Das[a)]
Department of Physics, Indian Institute of Technology, Powai, Mumbai 400076, India and Theoretical Physics Division, Bhabha Atomic Research Center, Mumbai 400085, India

(Received 19 November 2013; accepted 5 January 2014; published online 24 January 2014)

The effect of strongly coupled plasma on the ground state photoionization cross section is studied. In the non relativistic dipole approximation, cross section is evaluated from bound-free transition matrix element. The bound and free state wave functions are obtained by solving the radial Schrodinger equation with appropriate plasma potential. We have used ion sphere potential (ISP) to incorporate the plasma effects in atomic structure calculation. This potential includes the effect of static plasma screening on nuclear charge as well as the effect of confinement due to the neighbouring ions. With ISP, the radial equation is solved using Shooting method approach for hydrogen like ions (Li^{+2}, C^{+5}, Al^{+12}) and lithium like ions (C^{+3}, O^{+5}). The effect of strong screening and confinement is manifested as confinement resonances near the ionization threshold for both kinds of ions. The confinement resonances are very much dependent on the edge of the confining potential and die out as the plasma density is increased. Plasma effect also results in appearance of Cooper minimum in lithium like ions, which was not present in case of free lithium like ions. With increasing density the position of Cooper minimum shifts towards higher photoelectron energy. The same behaviour is also true for weakly coupled plasma where plasma effect is modelled by Debye-Huckel potential. © *2014 AIP Publishing LLC*.
[http://dx.doi.org/10.1063/1.4862550]

I. INTRODUCTION

Atomic physics[1–7] in hot dense plasma is one of the emerging fields of research in recent days. It has important applications in many fields of physics such as laser produced plasma, inertial confinement fusion (ICF), astrophysical systems, x-ray lasers, and plasma spectroscopy. The screening of nuclear charge due to the presence of additional charge distribution in plasma manifests as many interesting features in electronic properties of atoms or ions. Photoionization[8,9] is one of the properties of atoms or ions which exhibit significant changes due to the presence of plasma environment. Study of atomic photoionization cross section is essential in computing the radiative properties of plasma. Study of atomic processes[10] in plasma requires the knowledge of photoionization cross section of ions to estimate the charge state population. It plays important role in plasma diagnostic purpose also. Photoionization (PI) is very sensitive to detailed electronic structure of ions. The PI of isolated atomic system is a field pursued over for many decades. However, in recent days, considerable effort is being put in to understand the plasma effect on the PI cross section. The presence of external plasma environment alters the atomic potential experienced by the bound electrons, thereby affecting other electronic properties of ions. Though plasma free electrons as well as ions are responsible for the modification in the atomic potential, there exist no analytical expressions to account for the effects. Depending on the plasma conditions, i.e., density and temperature, model potentials are available to account for the effect of the plasma free electrons on the bound electrons via nuclear charge screening. Most popular model potentials[10] are Debye-Huckel potential and ion sphere potential. The choice of particular form depends on the plasma coupling parameter $\Gamma = \frac{E_{Coulomb}}{E_{thermal}} = \frac{Q^2}{4\pi\epsilon_0 a \kappa_B T}$, where Q is the charge on the particles, $a = (3/4\pi n)^{1/3}$ is the inter particle separation, n denotes plasma number density, and T is the temperature of plasma. In case of low dense and high temperature plasma, thermal energy dominates over the Coulombic interaction. Such kind of plasma is categorized as weakly coupled one for which $\Gamma < 1$. Debye-Huckel potential is the most widely used potential to obtain the electronic properties of ions in this kind of plasma. $\Gamma > 1$, however, corresponds to strongly coupled plasma (SCP)[11] which is generally having high density and low temperature. Sometimes, we can refer these systems as warm dense plasma. In such kind of plasma the coulomb interaction between plasma particles dominates over the thermal motion, and hence the ion motion is constrained in plasma having strong correlation. SCP is mostly encountered in ICF and laser produced plasma, dense astrophysical systems like interior of stars and jovian planets, etc. Recent technological progress has made it possible to create SCP systems in laboratory through laser ablation. Plasmas with $\Gamma > 1$ have been produced experimentally by fs laser pulse irradiation of the solid and thin foil targets. Laser ablation of matter can also produce short lived SCP where the plasma densities are close to solid mass densities at moderate temperatures ($T \sim 1$–10 eV). Recently, Ajai *et al.*[12] have succeeded in producing strongly coupled plasma with $\Gamma \sim 4$ using ns double pulsed laser ablation of lithium targets.

The adequate theoretical knowledge regarding various spectral properties like excitation energy, oscillator strength, transition properties, etc. is required for the proper diagnosis

[a)]Electronic mail: msdas@barc.gov.in

of SCP system. This study is also helpful for the estimation of radiative opacity of matter. Effect of dense plasma on the ionization potential, oscillator strength, collision and photo-absorption cross sections, fine structure splitting, spectral line shifts have been investigated earlier by many researchers.[13–17] A large community of atomic physicist use ion sphere potential to study the spectral properties of SCP system. In ISP, apart from static nuclear charge screening by electrons, the external confinement due to neighbouring ions also come into picture in an indirect manner through confining radius. Bhattacharya *et al.*[18] have used ISP to investigate the transition energies, oscillator strength, polarizability, etc. of hydrogen like C^{+5}, Al^{+13}, and Ar^{+17} ions using basis set expansion method.[18] Sen *et al.*[19] have applied the same methodology to obtain the polarizability and hyperpolarizabilities of hydrogen and helium like ions in a strongly coupled plasma system. Basu *et al.*[20] have studied dynamic polarizability of ions in dense plasma. Das *et al.*[22] have studied the effect of ion sphere plasma on various transition properties like excitation energy, oscillator strength, transition rate, etc. of li like C^{+3}, Al^{+10} using relativistic multi-reference Fock space coupled cluster method. In this work, we report our findings on the photoionization cross section of hydrogen and lithium like ions in SCPs.

The plasma environment has great effect on the photoionization cross section through the screening of long range electrostatic interaction. In case of weakly coupled plasma, the important manifestation of charge screening is appearance of shape resonances and Cooper minimum.[21] Shape resonances in the cross section appear due to the centrifugal barrier $l(l+1)/r^2$ where as Cooper minimum is a result of zeros in the bound-free transition matrix element. Detailed study of plasma effect on hydrogenic photoionization cross section is done by Lin *et al.*[25] and Qi *et al.*,[23,24] where they have observed sharp resonance peaks corresponding to transition to the quasi bound p states. Existence of Cooper minimum in lithium like ions is also revealed when the ion is subjected to Debye plasma.[26–28] However, very minimal work has been done in investigating the effect of strongly coupled plasma on photoionization dynamics. Only Jung *et al.*[29] have studied the K-shell photoionization of hydrogen like ion in strongly coupled plasma. In this paper, we aim at investigating the effect of strongly coupled plasma on hydrogen and lithium like systems. The strong confinement in ions has remarkable effect on the cross section through appearance of confinement resonances.[30–33] The plasma screening also results in appearance of Cooper minimum in lithium like ions and this phenomena is common to both weakly and strongly coupled plasma.

In this article, we discuss the photoionization cross section of hydrogen and lithium like ions embedded in strongly coupled plasma, described by ion sphere potential. The radial Schrodinger equation is solved for both bound and free states with IS potential. The Schrodinger equation is solved numerically using shooting method approach, where adaptive step size controlled Runge-Kutta method is employed to do the integration. Using the bound and continuum state wave functions, photoionization cross section is computed in non relativistic dipole approximation. The main findings of this investigation are occurrence of strong confinement resonances for low photoelectron energies. Cooper minimum is also observed in case of lithium like ions embedded in strongly coupled plasma. The paper is structured as follows. In Sec. II the computational methodology is discussed. Results and important findings are discussed in Sec. III. Finally conclusion is given in Sec. IV.

II. THEORY AND COMPUTATIONAL METHOD

The atomic photoionization cross section for $nl \rightarrow \epsilon l'$ transition in non relativistic dipole approximation ($l' - l = \pm 1$) is given by[34]

$$\sigma_{nl} = \frac{8\pi^2 \alpha a_0^2}{3(2l+1)}(\epsilon + I_{nl})[l R_{nl}^{\epsilon l-1^2} + (l+1)R_{nl}^{\epsilon l+1^2}], \quad (1)$$

where ϵ is the energy of photoelectron ejected from the ion, I_{nl} is the binding energy of nl state, $h\nu = I_{nl} + \epsilon$ represents the energy of the incident photon causing the radiative transition. Here,

$$R_{nl}^{\epsilon l\pm 1} = \langle P_{nl}|r|P_{\epsilon l\pm 1}\rangle = \int_0^\infty P_{nl}(r)\, r\, P_{\epsilon l\pm 1}(r)dr\,. \quad (2)$$

$P_{nl}(r)$ and $P_{\epsilon l}(r)$ represent the radial part of bound and continuum state wave functions which are obtained by solving the Schrodinger equation with appropriate potential $V(r)$. The equation can be written as follows:[35]

$$\frac{d^2P_{kl}(r)}{dr^2} + \left(2E_{kl} - 2V(r) - \frac{l(l+1)}{r^2}\right)P_{kl}(r) = 0. \quad (3)$$

Here $k = n$(principal quantum number) for bound states ($E_{nl} < 0$) and $k = \sqrt{2\epsilon}$ for continuum state ($E_{kl} = \epsilon > 0$ is the continuum state energy); l represents angular momentum quantum number; $P_{kl}(r)$ is the radial part of the wave function represented as $\Psi_{klm}(r,\theta,\phi) = \frac{P_{kl}(r)}{r}Y_m^l(\theta,\phi)$.

In case of a strongly coupled plasma, the potential $V(r)$ can be modelled using ion sphere approximation. Since the ion motion is strongly correlated, one can make the assumption that the ions are frozen in space. In this scenario, the whole plasma can be divided into non overlapping spherical volumes called ion sphere or Wigner-Seitz cell,[10] whose radius R_{IS} is given by

$$R_{IS} = (3/4\pi n)^{1/3}. \quad (4)$$

The ion sphere is made electrically neutral by assuming that each nucleus (Z) is surrounded by free electrons (Z_0) and the ionic core (Z–Z_0). In IS model, the effective potential felt by the bound electron can be represented as follows:[10]

$$V(r) = -\frac{Z}{r} + \frac{Z_0}{2R_{IS}}\left(3 - \frac{r^2}{R_{IS}^2}\right); \quad r < R_{IS}. \quad (5)$$

Because of strong confinement due to the neighbouring ions, we have chosen the vanishing boundary condition to be

satisfied at the boundary of ion sphere. This also adds to numerical simplicity. But, in reality, the bound state wave functions $P(r)$ in IS can extend out side the IS because of quantum tunnelling, which we have not considered here. The boundary and normalization conditions imposed on the bound state wave functions are given below

$$P_{nl}^{IS}(0) = 0; \quad P_{nl}^{IS}(r = R_{IS}) = 0$$
$$\int_0^{R_{IS}} P_{nl}^{IS}(r)^2 dr = 1. \tag{6}$$

Continuum state wave functions satisfy different normalization and boundary conditions. At origin, continuum state radial function $P_{\epsilon l}$ satisfies the same boundary condition as bound state functions but at $r \to \infty$, it exhibits asymptotic behaviour. The conditions are given as follows:[36]

$$P_{\epsilon l}(0) = 0,$$
$$P_{\epsilon l}(r \to \infty) \sim \sqrt{\frac{2}{\pi k}} \sin\left(kr - l\frac{\pi}{2} + \delta_\epsilon\right), \tag{7}$$
$$\int_0^\infty P_{\epsilon l} P_{\epsilon' l} dr = \delta(\epsilon - \epsilon').$$

Here, δ_ϵ represents the phase shift. Equation (3) is solved for bound states ($E_{nl} < 0$) and continuum states ($\epsilon > 0$) using the numerical methodology developed by Utsumi *et al.*[36] with proper boundary and normalization conditions. The details of the method are given in Ref. 36 and is not discussed here. In this approach, the second order boundary value problem is converted into coupled first order initial value problem and Shooting method approach is used to solve the coupled linear equations using the numerical integration techniques based on adaptive step size controlled Runge-Kutta method. Use of adaptive method for grid generation ensures lesser computational time as compared to uniform grid system. This method is a powerful tool to solve the free state wave functions. Here, highly oscillating continuum orbitals in far-field region are represented by phase-amplitude method ($P_{\epsilon l}(r) = y(r)\sin(\phi(r))$, where $y(r)$ and $\phi(r)$, respectively, represent amplitude and phase of the wave function. The main advantage of this method is that at each grid point we can get the value of radial function as well as their respective first derivative ($Q_{nl} = dP_{nl}(r)/dr$ and $Q_{\epsilon l} = dP_{\epsilon l}(r)/dr$) which can be directly used for evaluation of radial integrals using constrained interpolation polynomial (CIP) method as discussed in Ref. 36. Using the knowledge of energies and wave functions (bound and free), one can evaluate all other transition properties of ions in plasma. For our calculation, we have set the relative accuracy of 10^{-8} for energy convergence.

III. RESULTS AND DISCUSSION

Using the methodology of Utsumi *et al.*,[36] briefly described in Sec. II, we have solved the radial Schrodinger equation with ion sphere potential for hydrogen and lithium like ions for different plasma densities. The ground state energy level and $1s \to np$ transition energies for hydrogen like Al^{+12} ion in strongly coupled plasma is given in Table I. The values are compared with the data give in Ref. 18. The data in Ref. 18 are obtained by solving the energy eigenvalue equation using basis set expansion method. A very good agreement is seen between two sets of data. The ground state energies of hydrogen like lithium, beryllium, and carbon are also tabulated in Table II for plasma densities in the range 10^{16}–10^{25}/cc. It is observed that with increasing plasma density, the ground state energy levels move towards higher energy side and becomes unstable. This phenomenon in plasma physics community is commonly termed as continuum lowering. With further increase in density, the bound state merges into the continuum giving rise to phenomenon of pressure ionization. A comparison is also made with recently published data by Sen *et al.*[19] There is a very good agreement between both sets of data for Li^{+2} and C^{+5}. However, discrepancy arises for the case of Be^{+3}. In our case, the ionization potential ($|E_g|$) shows rapid decrease with increase in number density in contrast to the result reported by Sen *et al.* In their calculation, they have found that by changing the number density from 10^{16}/cc to 10^{24}/cc, the energy level exhibits no significant change.

TABLE I. IP and excitation energy of Al^{+12} for different R_{IS}.

R_{IS} (a.u.)	IP (a.u.)	IP[a] (a.u.)	$E_{1s\to2p}$ (a.u.)	$E_{1s\to2p}$[a] (a.u.)	$E_{1s\to3p}$ (a.u.)	$E^{a}_{1s\to3p}$ (a.u.)
9.9	82.6819	82.6819	63.3740	63.3740	75.1046	75.1048
5.7822	81.3875	81.3876	63.3700	63.3700	75.0784	75.0923
3.3814	79.1796	79.1796	63.3501	63.3501	74.9455	74.9801
3.1820	78.8466	78.8467	63.3451	63.3451	74.9117	74.9420
3.0227	78.5489	78.5489	63.3401	63.3401	74.8778	74.9037
2.8911	78.2784	78.2784	63.3351	63.3351	74.8441	74.8651
2.7798	78.0297	78.0297	63.3302	63.3301	74.8105	74.8261
2.6838	77.7987	77.7987	63.3252	63.3251	74.7774	74.7864
2.1301	76.061	76.061	63.2749	63.2749	74.5029	74.3137
1.9774	75.4113	75.4113	63.2496	63.2496	74.4187	74.0343
1.7676	74.3364	74.3364	63.1989	63.1985	…	…
1.4770	72.3462	72.3461	63.0728	63.0655	…	…
1.3419	71.1302	71.1306	62.9769	62.9492	…	…

[a]Bhattacharya *et al.*[18]

TABLE II. IP of Li^{+2}, Be^{+3}, C^{+5} for different plasma density.

	Li^{+2}		Be^{+3}		C^{+5}	
Plasma density (/cc)	E_g (a.u.)	E_g[a] (a.u.)	E_g (a.u.)	$E^a{}_g$ (a.u.)	E_g (a.u.)	$E^a{}_g$ (a.u.)
$\sim 10^{16}$	−4.4956	−4.4954	−7.99618	−8.0000	−17.99194	−17.988
1.0×10^{19}	−4.4562	−4.4562	−7.94268	−8.0000	−17.91942	−17.919
1.0×10^{20}	−4.4057	−4.4057	−7.87651	−8.0000	−17.8264	−17.826
1.0×10^{21}	−4.2970	−4.2969	−7.73399	−8.0000	−17.62601	−17.626
1.0×10^{22}	−4.0635	−4.0633	−7.42736	−7.9999	−17.19446	−17.194
5.0×10^{22}	−3.7571	−3.7553	−7.02271	−7.9999	−16.6234	−16.623
1.0×10^{23}	−3.5679	−3.5676	−6.77085	−7.9999	−16.26656	−16.266
5.0×10^{23}	−2.9249	−2.9244	−5.91727	−7.9998	−15.04437	−15.043
1.0×10^{24}	−2.4781	−2.4774	−5.39393	−7.9967	−14.28574	−14.284
5.0×10^{24}	…	…	−3.38478	−7.7133	−11.72897	−11.727

[a]Sen *et al.*[19]

Using the same methodology, wave functions for $l = 1$ partial waves in the energy range $0.0001 \leq \epsilon(a.u.) \leq 10$ are evaluated. The free state wave functions is most affected by the discontinuity in the potential appearing at the ion sphere boundary. The potential for different ion sphere radii corresponding to density range 10^{19}/cc to 10^{25}/cc of Li^{+2} is given in Fig. 1. The range and depth of the potential well varies with increasing density, i.e., decreasing ion sphere radius. The presence of edge at $r = R_{IS}$ in the potential affects the phase of the continuum state wave functions. The continuum p waves for $\epsilon = 0.0001$ a.u. for different radii are plotted in Fig. 2. The variation in the phase and amplitude of continuum wave functions due to confining potential have significant effect on the $1s \rightarrow \epsilon p$ transition matrix element.

Using the bound and continuum state wave functions, the matrix elements in Eq. (2) is computed for different photoelectron energies ϵ. The photoionization cross section which directly depends on the bound-free transition matrix elements is thus estimated. The photoionization cross section of Li^{+2} is depicted in Fig. 3 for $R_{IS} = 54.4313$ a.u. It corresponds to ion number density $\sim 10^{19}$/cc. Corresponding $\Gamma = \frac{\bar{Z}^2 e^2}{R_{IS} k_B T}$ is found out to be ~ 2 for 1 eV plasma. To ensure strong coupling we have considered the plasma temperature to be 1 eV through out our study. The photoionization cross section of hydrogenic systems is generally monotonically decreasing function of photoelectron energy. However, the PI cross section of hydrogen like lithium, as shown in Fig. 3, shows very different behaviour, particularly near the ionization threshold. At lower photoelectron energies, the cross section shows oscillations which die out at higher energies. At regime of higher photoelectron energy, the cross section obeys usual monotonically decreasing behaviour. The continuum p-waves are responsible for the occurrence of oscillations pertaining to the special form of the confining potential. The potential as given in Eq. (5) exhibits jump at the ion sphere boundary. This essentially gives rise to the oscillations, which are generally termed as "confinement resonances." People have earlier observed the confinement resonances in the photoionization cross section of confined hydrogenic systems. The confinement arising in form of potential barrier results in reflection of the continuum state wave functions. The constructive and destructive interference of continuum state wave functions with the reflected one results in the occurrence of confinement resonances. Higher energy continuum states are less affected by the confinement edge. This is the reason the oscillations tend to die

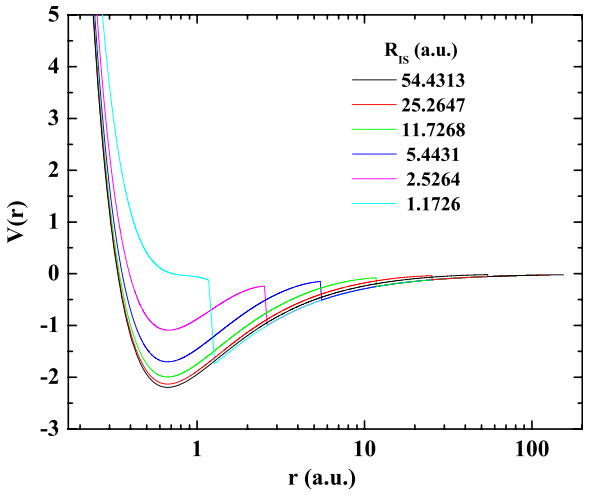

FIG. 1. Ion sphere potential of Li^{+2} ion for different R_{IS} ($\Gamma \sim 2$–92).

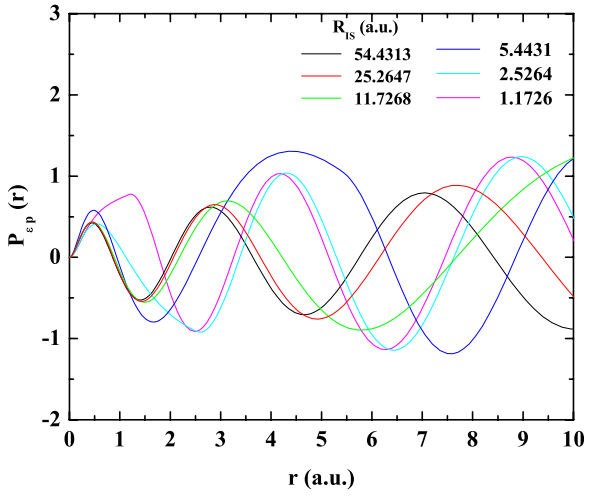

FIG. 2. p-wavefunction for different ion sphere radii of Li^{+2} ion ($\Gamma \sim 2$–92).

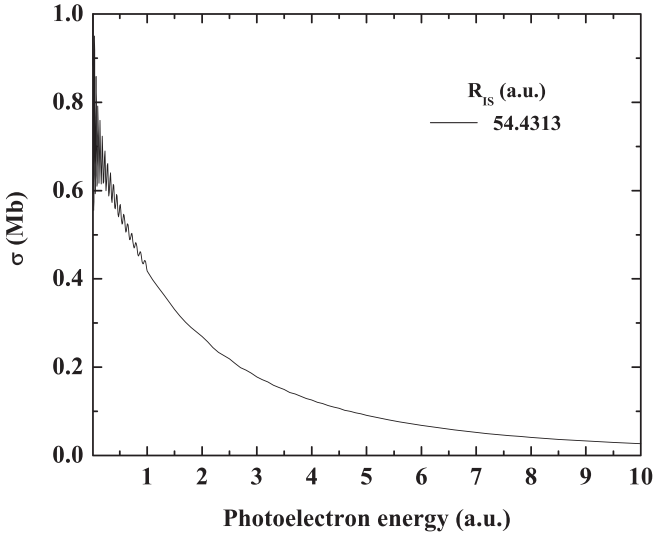

FIG. 3. Photoionization cross section of Li^{+2} ion plasma for ion density $\sim 10^{19}$/cc ($\Gamma \sim 2$).

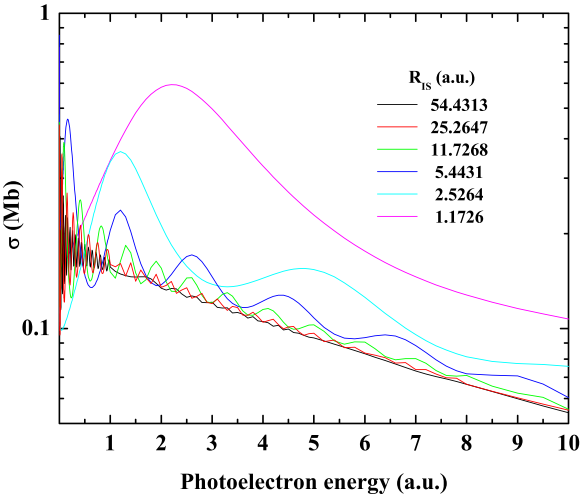

FIG. 5. Photoionization cross section of H like C^{+5} for different ion sphere radius ($\Gamma \sim 12$–580).

out for photoelectrons with high enough energy. The appearance of confinement resonances in the cross section is very much dependent on the edge of the confining potential. To investigate the issue, we have plotted, in Fig. 4, the PI cross section of Li^{+2} for different ion sphere radii corresponding to the ion number density in the range 10^{19}/cc to 10^{25}/cc. It can be seen that with decreasing ion sphere radius or in other words with increasing density, the vigorous oscillations in the cross section curve die out and the curve becomes smooth. At very high density we do not observe any oscillations in the cross section curve. The PI cross section for C^{+5} in the ion density regime 10^{19}/cc to 10^{25}/cc is also plotted in Fig. 5. It also behaves in a similar way. The strong confinement resonances near the ionization threshold are plotted in Fig. 6.

We have also investigated the behaviour of photoionization cross section of lithium like ions such as C^{+3}, O^{+5}, etc. subjected to strongly coupled plasma. An effective one electron potential $V_m(r)$ for the valance electron is chosen to account for the many electron core ($1s^2$) effects. Effective one e^- potential replaces the many electron interaction potential $V_{ee} = \sum_{i,j} \frac{1}{r_{ij}}$ with single particle function $V_m(r)$. It is based on the idea that the interaction of valance electron with the multi-electron core can be represented by modified coulomb potential. In the limit of large r, $V_m(r)$ simply represents Coulomb potential created by the ion and at origin $r = 0$ it represents the potential created by nuclear charge Z. The effective one electron potential for an ion with nuclear charge Z and ionization state $\bar{Z}$ then satisfies following properties:

$$\lim_{r\to\infty} V_m(r) = -\frac{\bar{Z}}{r}, \tag{8}$$

$$\lim_{r\to 0} V_m(r) = -\frac{Z}{r}. \tag{9}$$

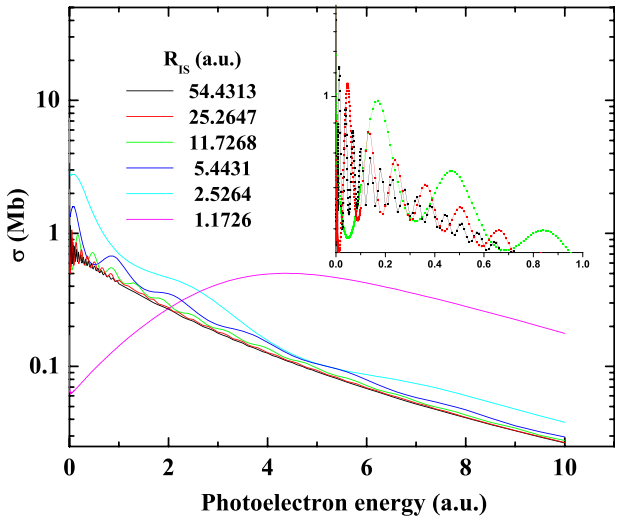

FIG. 4. Photoionization cross section of Li^{+2} ion plasma for different ion sphere radii ($\Gamma \sim 2$–92). Inset shows the magnified portion of curve near the ionization threshold.

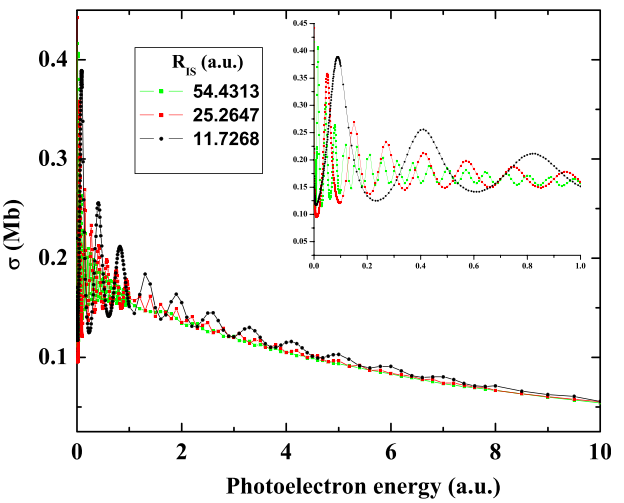

FIG. 6. Strong confinement resonances in the photoionization of C^{+5} ion ($\Gamma \sim 12$–57). Inset shows the magnified portion of the curve near the ionization threshold.

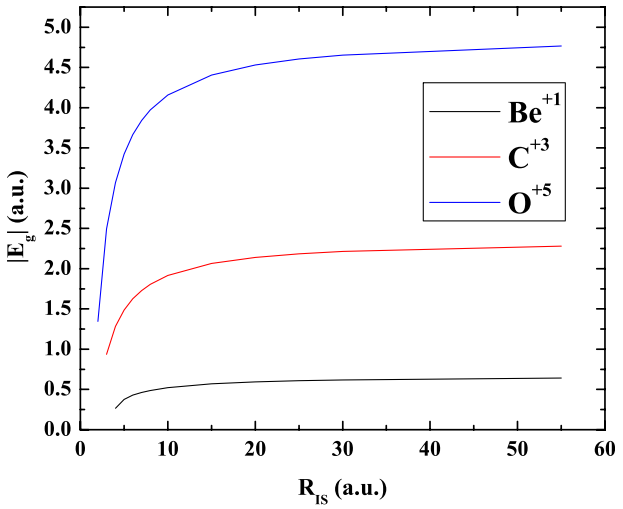

FIG. 7. Variation of 2*s* state energy of lithium like Be, C, O ions with ion sphere radius.

$\bar{Z} = 1, 2, 3\ldots$. represent, respectively, neutral atom, singly ionized ion, doubly ionized ion, etc. The form of the model potential as used in our work is given by[37]

$$V_m(r) = -\frac{1}{r}\left[\bar{Z} + (Z - \bar{Z})e^{-a_1 r} + a_2 r e^{-a_3 r}\right]. \qquad (10)$$

The potential contains exponential terms which are used to simulate the electron-electron repulsion in multi-electron core with Coulomb singularity only. a_1, a_2, and a_3 are model potential parameters which are optimized to give correct energy eigenvalues of the atomic system. For Li like Be^{+1}, C^{+3}, O^{+5}, the parameters are, respectively, $[a_1 = 4.733, a_2 = 4.804, a_3 = 4.814]$, $[a_1 = 7.655, a_2 = 7.654, a_3 = 7.674]$, and $[a_1 = 10.467, a_2 = 10.449, a_3 = 10.552]$. The ground state energy for different ion sphere radius is plotted in Fig. 7. The ground state energy corresponding to different ion sphere radius is also tabulated in Table III. Here also we can see the lowering of ip with decreasing ion sphere radius.

After investigating the ground state behaviour, we have computed the bound-free transition matrix element using Eq. (2) and subsequently photoionization cross section is computed using Eq. (1). The cross section plot for C^{+3} is given in Fig. 8. Confinement resonances are also observed near the ionization threshold at low densities. Apart from confinement resonances, the effect of strongly coupled plasma manifests itself in form of Cooper minimum, where the photoionization cross section drops to zero. Cooper minimum is resulted from the zeros in the transition matrix element. This kind of behaviour is characteristic of atoms having at least one node in outer valance shell except 2 s shell. It is worth noting that all alkali metal atoms except lithium contain Cooper minimum in the ground state photoionization cross section in their free state.[38–40] However, when the lithium like ion is embedded in strongly coupled plasma, the Cooper minima are revealed. The same behaviour is also true for a weakly coupled plasma. The occurrence of Cooper minimum in Li like ions subjected to plasma environment is solely due to the plasma density and temperature. Essentially, the perturbation in the micro-field around the ion results in variation of phases and amplitudes of overlapping bound and free state wave functions. For certain plasma condition, the positive and negative components of the oscillatory bound and continuum states just cancel each other leading to zero in the dipole matrix element. The Cooper minimum appearing in C^{+3} is separately plotted in Fig. 9. In C^{+3} the minimum starts appearing at $R_{IS} = 3$ a.u., i.e., for ion number density $\sim 10^{23}$/cc. It can also be seen that with increasing density, i.e., decreasing confinement radius, the Cooper minimum starts moving towards higher photoelectron energies. The low energy hump following Cooper minimum also decreases with increasing density. The Cooper minimum occurring in O^{+5} is also plotted in Fig. 10. In this case minimum appears for ion density $\sim 3 \times 10^{23}$/cc. Here also, the Cooper minimum follows the same trend as in C^{+3}. The ground state energy as well as the location of Cooper minimum for C^{+3} and O^{+5} are plotted in Fig. 11. With decreasing ion sphere radius, the ground state becomes more and more unstable and finally at some point merges into continuum. As the ground state moves towards the ionization threshold, the overlap decreases leading to reduced

TABLE III. Ground state energy E_g of Li like system for different ion sphere radius R_{IS} (E_g and R_{IS} are in atomic units).

R_{IS}	Be^{+1}	C^{+3}	O^{+5}
55	−0.64096	−2.28157	−4.76787
30	−0.61832	−2.21348	−4.65431
25	−0.6084	−2.18356	−4.60437
20	−0.59359	−2.13873	−4.52952
15	−0.5691	−2.06422	−4.40495
10	−0.52124	−1.91624	−4.15669
8	−0.48654	−1.80648	−3.97155
7	−0.46217	−1.72889	−3.84001
6	−0.42888	−1.6267	−3.6657
5	−0.37581	−1.48647	−3.42409
4	−0.26662	−1.28239	−3.06819
3		−0.93826	−2.49608
2			−1.34747

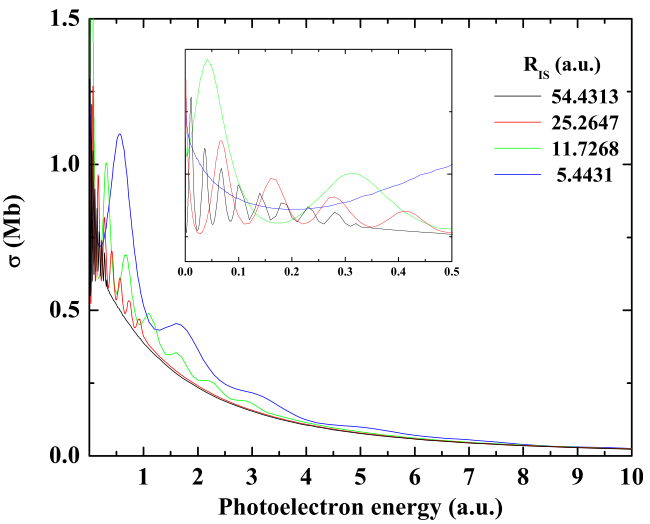

FIG. 8. Confinement resonances in C^{+3} photoionization cross section due to strongly coupled plasma effect ($\Gamma \sim 4$–44).

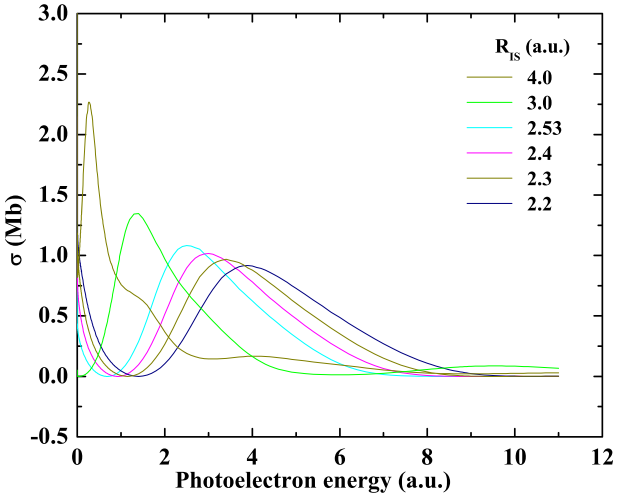

FIG. 9. Appearance of Cooper minimum in the photoionization cross section of C^{+3} ion ($\Gamma \sim 61$–111).

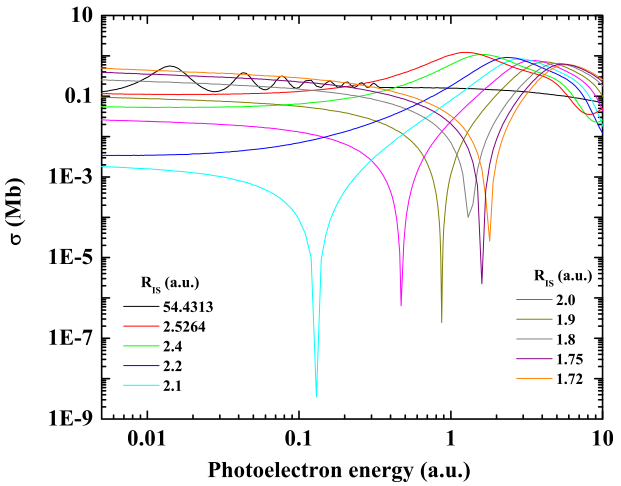

FIG. 10. Confinement resonance and Cooper minimum in photoionization cross section of O^{+5} ion in SCP ($\Gamma \sim 12$–580).

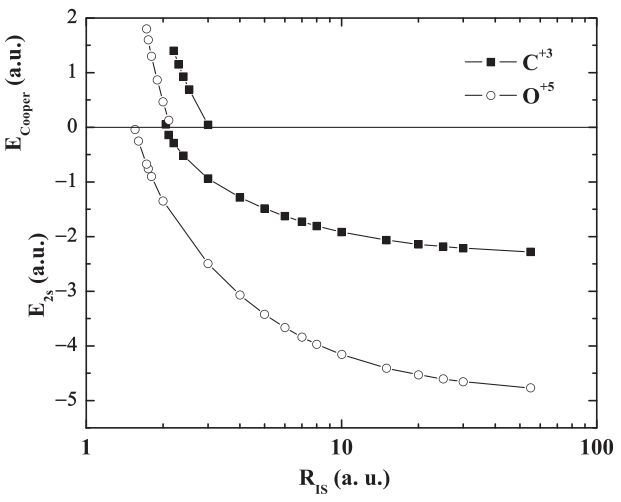

FIG. 11. Ground state instability and position of Cooper minimum in C^{+3} and O^{+5} ions.

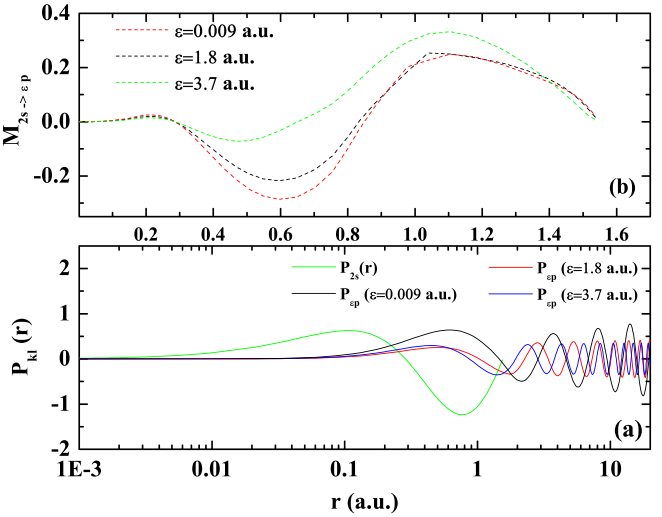

FIG. 12. (a) Radial wave function for 2 s state and continuum states with $\epsilon = 0.009$, 1.8, 3.7 a.u. (b) $\int_0^{R_{IS}} P_{2s} r P_{\epsilon p} dr$ for $\epsilon = \epsilon = 0.009$, 1.8, 3.7 a.u.

cross section at the threshold. Finally at some density Cooper minimum starts appearing. To investigate this issue we have plotted, in Fig. 12(a), the 2 s wave function and continuum p waves for $\epsilon = 0.009$, 1.8, 3.7 a.u. of O^{+5} for $R_{IS} = 1.72$ a.u. It can be seen that the in the range of the bound state wave function, the continuum wave functions for different energies have got different amplitudes and phases. Thus, at some energy the continuum wave function behaves in such a manner that the positive and negative amplitudes exactly cancel each other leading to Cooper minimum. The dipole matrix elements $M_{2s\to\epsilon p} = \int_0^{R_{IS}} P_{2s} r P_{\epsilon p} dr$ is plotted in Fig. 12(b). It is observed that for photoelectron energy 1.8 a.u., the positive and negative amplitudes exactly cancels each other leading to Cooper minimum. However, at energies away from it, there is net residual overlap between the bound and continuum states. Its location in the photoelectron energy range moves away from threshold with increasing density which is depicted in Fig. 11.

There exists no previous data for comparison with our calculation. However, Baltenkov *et al.*[31] have studied the photoionization cross section of hydrogen like ions surrounded by charged spherical shell. They have also observed the confinement resonances in the cross section curve. Similarly, Lin *et al.*[32] have investigated the cross section of hydrogen and lithium like ions in power exponential potential. They have observed confinement resonances for potentials having sharp edge. In case of potential having smooth boundary, resonance structure in the cross section disappears. Our results can be qualitatively compared with these results.

IV. CONCLUSION

The effect of strongly coupled plasma on the ground state photoionization cross section of ions is investigated here. The plasma effect in this case is modeled via ion sphere potential and the radial Schrodinger equation is solved using Shooting method approach. We have observed confinement resonances in the photoionization cross section in hydrogen

like ions such as Li^{+2}, C^{+5}, etc. near the ionization threshold. The confinement resonances appear due to the constructive and destructive interference of continuum wave function with the wave that gets reflected from the edge of the ISP. The resonances start disappearing with increasing density of the system. Similarly, lithium like ions such as C^{+3}, O^{+5}, etc. also exhibit confinement resonances. Another interesting feature of lithium like ions is that it contains Cooper minimum when subjected to plasma environment. Free Li like ions do not contain any Cooper minimum in the cross section curve. The Cooper minimum starts moving towards higher photoelectron energies with decreasing ion sphere radius.

It is to emphasize that we have studied the effect of static screening on the photoionization cross section. The static screening approximation takes into account the average interaction between plasma particles and ionic bound electrons. This approximation is valid in a plasma where the interaction time between the charge particles is more than the plasma response time. In certain cases the dynamic screening (DS) effect has to be taken into account in order to describe the instantaneous correlation between the ion and projectile plasma particles. Collective plasma oscillations can also play important role in high dense plasma. The DS effect as well as plasma fluctuations can be described by plasma dielectric constant which is a measure of polarization of the plasma electric field. Using dielectric constant, people have studied the DS effect of approaching projectile electron on the electron impact excitation.[41–44] However, DS effect on photoionization cross section is still open field. As pointed out by many authors, DS may have significant effect in a highly dense plasma or for excitations involving lower photon energies. The low energy excitations are most affected in SCP where we observe resonance structures. Dynamic screening effect may play important role in this regime. However, we expect that inclusion of dynamic screening will not change the overall behaviour of photoionization cross section obtained for static screening case. Detail investigation along this line is required to properly quantify the effect.

Drastic changes observed in the photoionization cross section in a strongly coupled plasma can have overall effect on the radiative properties of system. Our study can be useful in this regard. More research in this direction is called for to validate the results.

ACKNOWLEDGMENTS

Authors would like to thank Dr. N. K. Gupta, BARC for his encouragement. We are also thankful to the anonymous reviewer for the useful comments.

[1]C. Gao, J. Zeng, and J. Yuan, High Energy Density Phys. **7**, 54 (2011).
[2]J. Pang, G. Han, Z. Q. We, and S. C. Li, J. Phys. B: At. Mol. Opt. Phys. **35**, 2117 (2002).
[3]Y. Li, J. Wu, Y. Hou, and J. Yuan, J. Phys. B: At. Mol. Opt. Phys. **41**, 145002 (2008).
[4]D. Ray, Phys. Rev. E **63**, 027401 (2000).
[5]T. C. Killian, T. Pattard, T. Pohl, and J. M. Rost, Phys. Rep. **449**, 77 (2007).
[6]B. Saha, P. K. Mukherjee, D. Bielinska-Waz, and J. Karwowski, J. Quant. Spectrosc. Radiat. Transfer **92**, 1 (2005).
[7]B. Saha and S. Fritzsche, Phys. Rev. E **73**, 036405 (2006).
[8]A. F. Starace, *Photoionization of Atoms* (Anthony F. Starace Publication, 1996).
[9]J. J. Yeh and I. Lindau, At. Data Nucl. Data Tables **32**, 1 (1985).
[10]D. Salzman, *Atomic Physics in Hot Dense Plasma* (Oxford University Press, New York, 1998).
[11]S. Ichimaru, Rev. Mod. Phys. **54**, 1017 (1982).
[12]A. Kumar, V. Sivakumaran, J. Ashwin, R. Ganesh, and H. C. Joshi, Phys. Plasmas **20**, 082708 (2013).
[13]J. C. Stewart, Jr. and K. D. Pyatt, Astrophys. J. **144**, 1203 (1966).
[14]B. F. Rozsnyai, Phys. Rev. A **43**, 3035 (1991).
[15]D. Ray, Phys. Rev. E **62**, 4126 (2000).
[16]Y. D. Jung, Eur. Phys. J. D **7**, 249 (1999).
[17]H. R. Griem, Phys. Rev. A **38**, 2943 (1988).
[18]S. Bhattacharyya, A. N. Sil, S. Fritzsche, and P. K. Mukherjee, Eur. Phys. J. D **46**, 1 (2008).
[19]S. Sen, P. Mandal, P. K. Mukherjee, and B. Fricke, Phys. Plasmas **20**, 013505 (2013).
[20]J. Basu and D. Ray, Phys. Rev. E **83**, 016407 (2011).
[21]S. T. Manson, Phys. Rev. A **31**, 3698 (1985).
[22]M. Das, M. Das, R. K. Chaudhuri, and S. Chattopadhyay, Phys. Rev. A **85**, 042506 (2012).
[23]Y. Y. Qi, J. G. Wang, and R. K. Janev, Eur. Phys. J. D **63**, 327 (2011).
[24]Y. Y. Qi, J. G. Wang, and R. K. Janev, Phys. Rev. A **80**, 063404 (2009).
[25]C. Y. Lin and Y. K. Ho, Phys. Plasmas **17**, 093302 (2010).
[26]C. Y. Lin and Y. K. Ho, Phys. Rev. **81**, 033405 (2010).
[27]Y. Y. Qi, Y. Wu, and J. G. Wang, Phys. Plasmas **16**, 033507 (2009).
[28]S. Sahoo and Y. K. Ho, Phys. Plasmas **13**, 063301 (2006).
[29]Y. D. Jung, Phys. Plasmas **5**, 4456 (1998).
[30]V. K. Dolmatov and S. T. Manson, Phys. Rev. A **73**, 013201 (2006).
[31]A. S. Baltenkov, S. T. Manson, and A. Z. Msezane, Phys. Rev. A **76**, 042707 (2007).
[32]C. Y. Lin and Y. K. Ho, J. Phys. B: At. Mol. Opt. Phys. **45**, 145001 (2012).
[33]V. K. Dolmatov, A. S. Baltenkov, J. P. Connerade, and S. T. Manson, Rad. Phys. Chem. **70**, 417 (2004).
[34]H. A. Bethe and E. E. Salpeter, *Quantum Mechanics of One and Two-Electron Atoms* (Academic, New York, 1957).
[35]B. H. bransden and C. J. Joachain, *Physics of Atoms and Molecules* (Pearson Education, Singapore, 2004).
[36]T. Utsumi and J. Koga, Comput. Phys. Commun. **148**, 267 (2002).
[37]W. Schweizer, P. Fabinder, and R. G. Lez-Ferez, At. Data Nucl. Data Tables **72**, 33 (1999).
[38]G. McGinn, J. Chem. Phys. **53**, 3635 (1970).
[39]J. A. Tully, Astrophys. J. **288**, 831 (1985).
[40]R. E. H. Clark, R. D. Cowan, and F. W. Bobrowicz, At. Data Nucl. Data Tables **34**, 415 (1986).
[41]Y. D. Jung, Phys. Rev. E **55**, 3369 (1997).
[42]Y. D. Jung, Phys. Plasmas **5**, 536 (1998).
[43]C. G. Kim and Y. D. Jung, Phys. Plasmas **5**, 3493 (1998).
[44]M. S. Murillo and J. C. Weisheit, Phys. Rep. **302**, 1 (1998).